Received: 6 June 2023 | Revised: 9 November 2023 | Accepted: 27 November 2023

IET Quantum Communication

DOI: 10.1049/qtc2.12081

The Institution of Engineering and Technology WILEY

ORIGINAL RESEARCH

Quantum BER estimation modelling and analysis for satellite-based quantum key distribution scenarios

Abhishek Khanna | **Sambuddha Majumder** | **Adarsh Jain** | **Dinesh Kumar Singh**

Space Applications Centre, ISRO, Ahmedabad, India

Correspondence
Abhishek Khanna.
Email: akn@sac.isro.gov.in

Abstract

The quantum communication channel is considered to be eavesdropped when the signal Quantum Bit Error Rate (QBER) exceeds a defined theoretical limit and is thus considered a figure of merit parameter for assessing the security of a quantum channel. This work presents a general mathematical model considering device imperfections and various sources of errors for estimating signal QBER in polarisation encoded satellite-based QKD systems. QBER performance for satellite-to-ground downlink scenarios has been investigated for multiple sky brightness conditions (day time and night time operations), two operating wavebands: 800 and 1550 nm as well as for different quantum transmitter and quantum receiver architectures. Further, a novel QBER estimation analysis for inter-satellite QKD links has also been presented. The estimation results obtained from the developed model have been validated against and found in good agreement with the measured results of the only reported satellite-to-ground QKD experiments till date. The presented QBER modelling and analysis will aid in system engineering and efficient design of future satellite-based QKD systems.

KEYWORDS
private key cryptography, quantum communication, quantum cryptography

1 | INTRODUCTION

Quantum Key Distribution (QKD) is a technique to ensure unconditional secure key distribution between two parties by using the principles of quantum mechanics [1]. Developed by Bennet and Brassard in 1984 [2], the first experiment was conducted eight years later using a 32 cm free space transmission [3, 4]. QKD has come a long way since then with several experiments leading to a lot of new free space and fibre-based QKD protocols using different encoding schemes like polarisation, phase and time-bin over much larger distances. This quantum evolution has led to a large boost in the related technologies such as single photon sources [5], single photon detectors [6], time taggers etc. along with several advancements in post processing techniques such as error correction and privacy amplification.

Due to absorption in fibre cables and atmospheric losses, fibre and terrestrial free space QKD are limited to few hundreds of kilometres [7, 8]. However, the satellite-based free space QKD link can overcome such limitations by successfully distributing secure keys between two ground stations situated over thousands of kilometres apart. Several space agencies are working towards the establishment of satellite-to-ground quantum communication links [9–16]. The two standard operating wavelengths window suitable for space-based quantum communication are 800 and 1550 nm. The former wavelength is preferred because of the availability of efficient and low-cost detector technology, while the latter is better suited for realising all day-time operational QKD links.

The quantum bit error rate or QBER is considered as an important figure of merit for polarisation encoded QKD systems for analysing the security of a quantum communication

Abbreviations: FOV, Field of View; ISL, Inter-Satellite Link; LEO, Low Earth Orbit; OGS, Optical Ground Station; QBER, Quantum Bit Error Rate; QKD, Quantum Key Distribution.

channel. The quantum channel is considered to be eavesdropped when the QBER exceeds the value of 11% [17] and would not be able to generate any secure keys for encryption. The accurate error and link loss estimation are therefore essential to efficiently analyse and optimally design the satellite-based QKD links. The currently available literature [14, 18–21] quantifying the errors in a satellite-based QKD link lacks in comprehensive analysis and modelling of the signal QBER considering various quantum transmitter and receiver design parameters. Also, to the best of our knowledge, none of the reported papers address the QBER estimation for the ISL-QKD scenario.

In this work, we have presented a simple mathematical model to obtain the QBER of a polarisation encoded satellite-based quantum communication system by analysing the errors introduced due to the free space transmission channel and limitation of the quantum transmitter and receiver. The major constituents responsible for limiting the noise performance are stray light, polarisation errors as well as dark noise and after-pulsing effects of the detectors. This developed model is then used to analyse the satellite-to-ground quantum communication link in a downlink configuration and inter-satellite (ISL) QKD link for 800 nm as well as 1550 nm wavebands. The QBER is analysed for different sky brightness situations such as clear daytime, full moon clear night and moonless clear night. The detailed comparative analysis is then presented to aid in the design of an efficient satellite QKD system.

This paper is organised as follows: the mathematical modelling of the QBER is presented in Section 2. In Section 3, the analysis of the satellite-to-ground QKD scenario is done followed by the analysis of the ISL QKD in Section 4. In section 5, the system requirements for practical and efficient realisation of satellite-based QKD scenarios are presented. Finally, we conclude the work in Section 6.

2 | QBER MODEL

The QBER of a quantum communication channel accounts for the errors in the link and is defined as the ratio of the number (or rate) of wrong bits to the number (or rate) of total received bits.

$$QBER = \frac{N_{wrong}}{N_{wrong} + N_{right}} = \frac{R_{wrong}}{R_{wrong} + R_{right}} \quad (1)$$

Figure 1 illustrates the schematic of a polarisation-based QKD receiver which includes key components such as half-wave plates, single photon detectors (SPD) band pass filters ($\Delta\lambda$), 50/50 beam splitter (BS), polarisation beam splitters (PBS), waveplate-based polarisation compensator (PC) and the primary sources of noise in a BB84 QKD optical receiver. A satellite-based QKD scenario is prone to different noise factors introduced due to dark count (N_{dc}), stray light (N_{stray}), polarisation errors (N_{SOP}) and after-pulsing (N_{AP}). N_{wrong} can be defined as follows:

$$N_{wrong} = N_{dc} + N_{stray} + N_{SOP} + N_{AP} \quad (2)$$

In this work, we have considered a polarisation encoded 2-state decoy BB84 QKD protocol given its suitability in satellite-based QKD scenarios in terms of high secure key rate, longer transmission distance and robust eavesdropper detection [22]. However, for the practical implementation of this protocol, one of the critical parameters of importance is s, the occurrence percentage or proportion of signal pulses against decoy and vacuum pulses at the Quantum transmitter output and has implications on the signal bits generated at the ground and hence overall QBER. Thus, a more generic QBER (E_μ) expression in the high-loss regime also incorporating this parameter can be represented as follows:

$$E_\mu = \frac{e_o Y_o + e_{pol} \times \left(1 - e^{-(t_{link} \times \mu \times s)}\right)}{Q_\mu} \quad (3)$$

where $Q_\mu = Y_o + \left(1 - e^{-(t_{link} \times \mu \times s)}\right)$ is the defined as the gain of the signal states. μ is the signal mean photon number, e_o is the error rate due to the random background noise and is considered as 0.5. The term $(1\text{-}e^{-(t_{link} \times \mu \times s)})$ expresses the detection probability due to incoming photons from a signal state. e_{pol} is the probability of incorrect bit received due to the

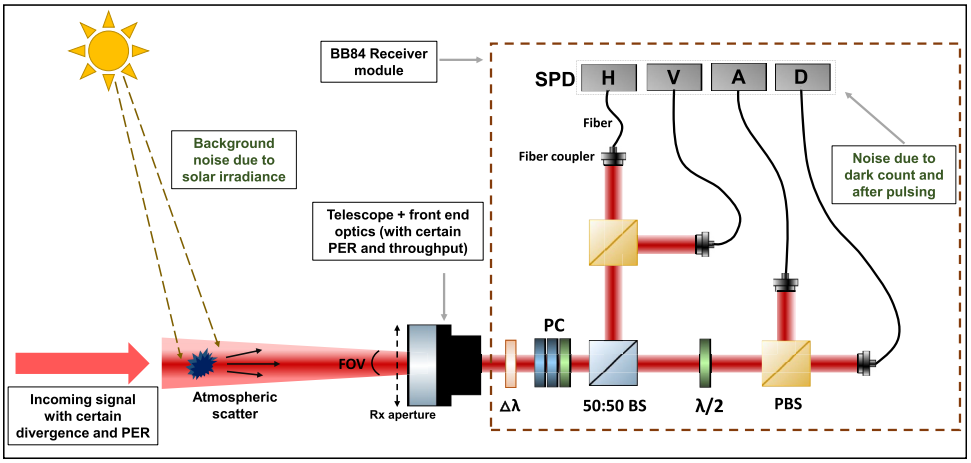

FIGURE 1 Schematic illustrating key components and noise contributions in a polarisation-based QKD receiver.

polarisation errors and can be calculated using the phase delay and basis deviation [23] as follows:

$$e_{pol} = \frac{1}{(ER+1)} + \frac{(ER-1)}{(ER+1)}\sin^2(\theta) \quad (4)$$

here θ corresponds to basis deviation, and ER represents the signal's Polarisation Extinction Ratio. Yo, the background detection probability is represented by

$$Yo = \left(4d \times \Delta t + N_{stray} \times \eta_{\text{op}} \times \eta_{\text{qrx}}\right) \quad (5)$$

Here, the first term represents the noise contribution due to dark counts of single photon detectors. It depends on the detector dark count rate (d) and the gating window (Δt). Here, the time gate filtering is applied to reduce the number of background photons.

The second term corresponds to the noise due to stray light. N_{stray} represents the number of stray photons per pulse, which is directly related to the brightness conditions of the sky and other receiver optics properties such as telescope aperture size, field of view (FOV) and receiver spectral filter bandwidth B_{filter}. η_{op} corresponds to the quantum receiver terminals front end optics throughput, and η_{qrx} corresponds to the quantum receiver efficiency including free space to fibre coupling, which is related to the receive chain architecture. The stray noise power received by the telescope can be given as [18] follows:

$$P_b = H_b \times \Omega_{FOV} \times A_{rx} \times B_{filter} \quad (6)$$

where H_b is the brightness of the sky background in $W.m^{-2}.Sr^{-1}.nm^{-1}$. Ω_{FOV} is the quantum receiver field of view in a solid angle, and A_{rx} is the receive telescope aperture area. Thus, by choosing different values of lighting and weather conditions (H_b) and different properties of the optics, we can obtain the noise received in different satellite-to-ground QKD scenarios. Using this P_b, we can therefore calculate the number of undesired photons received per pulse for a given detector:

$$N_{stray} = \frac{P_b}{h\upsilon}\Delta t \quad (7)$$

The t_{link}, probability of a photon being detected at the receiver or the total link efficiency can be expressed as a product of several loss factors:

$$t_{link} = \eta_{geo} \times \eta_{atm} \times \eta_{point} \times \eta_{op} \times \eta_{qrx} \quad (8)$$

η_{geo} corresponds to the geometric loss factor and can be represented as [24] follows:

$$\eta_{\text{geo}} = \left[\frac{D_{rx}}{D_{tx} + Div \times R}\right]^2 \quad (9)$$

D_{tx} and D_{rx} corresponds to the transmitter and receiver aperture diameter respectively, R represents the slant range and Div corresponds to the estimated divergence of the transmitter telescope. The divergence can be estimated by multiplying the theoretical divergence by a factor (greater than 1), so as to account for any practical limitation (taken 1.2 in this work). η_{atm} corresponds to the atmospheric loss factor and is calculated from an atmospheric loss of 1–4 dB for 1550 nm and 2–5 dB for 785 nm [25] with OGS visibility elevation angles ranging from 30° to 90°. η_{point} represents the loss factor due to the error in the beam pointing.

Another factor that needs to be accounted for is the after-pulsing phenomena which represents the spontaneous detection events being triggered by trapped carriers after previous avalanches at the detector [26]. It depends on the detector after-pulsing probability (P_{AP}) and the number of detector clicks generated from different sources. For commercially available SPAD, the after-pulsing probability reported can be as large as 3%. This will cause a non-trivial increase in QBER and thus necessitates its incorporation in the overall noise error counts. Therefore, to arrive at a general expression for the estimation of signal QBER, eq (3) can be further modified as folllows:

$$E_\mu = \frac{e_o \times Y'_o + \left(e_{pol} + e_o \times P_{AP}\right) \times \left(1 - e^{-(t_{link} \times \mu \times s)}\right)}{Y'_o + \left(1 - e^{-(t_{link} \times \mu \times s)}\right) \times \left(1 + (P_{AP})\right)} \quad (10)$$

where Y'_o is expressed as $Y_o(1+P_{AP})$, which includes the erroneous counts due to after pulsing caused by the detection events of stray light and dark counts.

3 | SATELLITE-TO-GROUND QUANTUM LINK

For a satellite-to-ground QKD scenario, a satellite at a typical circular LEO orbit with an altitude of 500 km with an inclination of 31° is chosen for analysis. For Optical Ground Station (OGS), a visibility elevation of 30° is chosen so as to account for the completion of the pointing and acquisition phase. As a result, the maximum and minimum range for a typical satellite overhead pass over the OGS lies within 900–500 km. For this analysis, the worst-case slant range, that is, the maximum range of 900 km is considered for various loss calculations. The pointing loss is taken as 3 dB as this is acceptable for the required limits of receiver FOV. The front-end optics consist of the telescope and the relay optics and is assumed to have a throughput of ~75%.

The receiver efficiency is taken as ~50% that includes the total efficiency of the detector, fibre coupling and associated losses of the BB84 decoding module. The dark count rate per detector is taken as 100 Hz, while the after pulse probability for 785 nm is taken to be 2% for a Single Photon Avalance Diode (SPAD)-based single photon detector [28], while for 1550 nm, it is considered zero as SNSPD (Superconducting Nanowire Single Photon Detector) types of detectors [29] are used. Ultra-narrow bandpass filters with a filter bandwidth B_{filter} of 0.2 nm [30] are considered for analysis. For the stray

light calculation, three different cases have been considered with values of H_b [18, 25, 27] as given in Table 1. The other system specifications chosen for the satellite-to-ground scenario include the transmitter aperture diametre (100–300 mm), the receiver aperture diameter (1000 mm), polarisation error (1%) and detector gating window (1.25 ns). The same analysis can be extended for other orbits and subsystem properties as per the user requirements.

In Figure 2, the QBER is calculated for both the wavelengths at three different sky brightness conditions, that is, moonless night, moonlit night and clear day. Firstly, for the moonless night scenario, with smaller receiver FOV values and assuming the pointing loss would still be less than 3 dB, the QBER is primarily dominated by error counts due to the after pulsing of the detector, and as a result, 1550 nm has a better SNR performance given the absence of after pulsing effects. However, as the FOV increases, the QBER due to the stray noise dominates. Since the number of noise photons per pulse at moonless night for 1550 nm is more due to smaller energy per photon, the QBER increases rapidly as the FOV is increased, while for 785 nm, we can achieve acceptable signal QBER even with comparably larger FOVs. For the case of moonlit night and clear day, the stray noise at 1550 nm is expected to be lesser than 785 nm [18, 25, 27], leading to a decrease in error counts at 1550 nm. Therefore, as the FOV increases, the QBER for 785 nm increases more quickly. However, for clear day-conditions, the FOV specifications become very stringent even with a 300 mm onboard Tx telescope aperture, leading to very fine pointing requirements.

4 | QUANTUM ISL LINK

For the ISL scenario, up-conversion detectors are considered for the receiver at 1550 nm having an overall photon detection efficiency typically as 30% and a dark count rate of ≤150 cps with the after pulsing of ~1% [31–33]. The aperture of both the transmitter and receiver telescopes is assumed to have the same diametre. The signal QBER is calculated for varying ISL separation between the two satellites and different transmit apertures as plotted in Figure 3. Here, we are considering only the case when both the satellites are in eclipse as sufficient ISL contact time is available to perform QKD even when both the satellites are in complete darkness. Therefore, for a typical 500 km orbit and ISL separation of ~1000 km, the satellites will have as high as ~8.5 h/day access duration.

TABLE 1 Typical radiance data for 785 and 1550 nm[18, 25, 27].

Atmospheric condition	Hb ($W.m^{-2}.Sr^{-1}.nm^{-1}$) 785 nm	Hb ($W.m^{-2}.Sr^{-1}.nm^{-1}$) 1550 nm
Clear day	3.1×10^{-3}	6.85×10^{-5}
Moonlit clear night	1.5×10^{-6}	1.5×10^{-7}
Moonless clear night	1.5×10^{-8}	1.5×10^{-8}

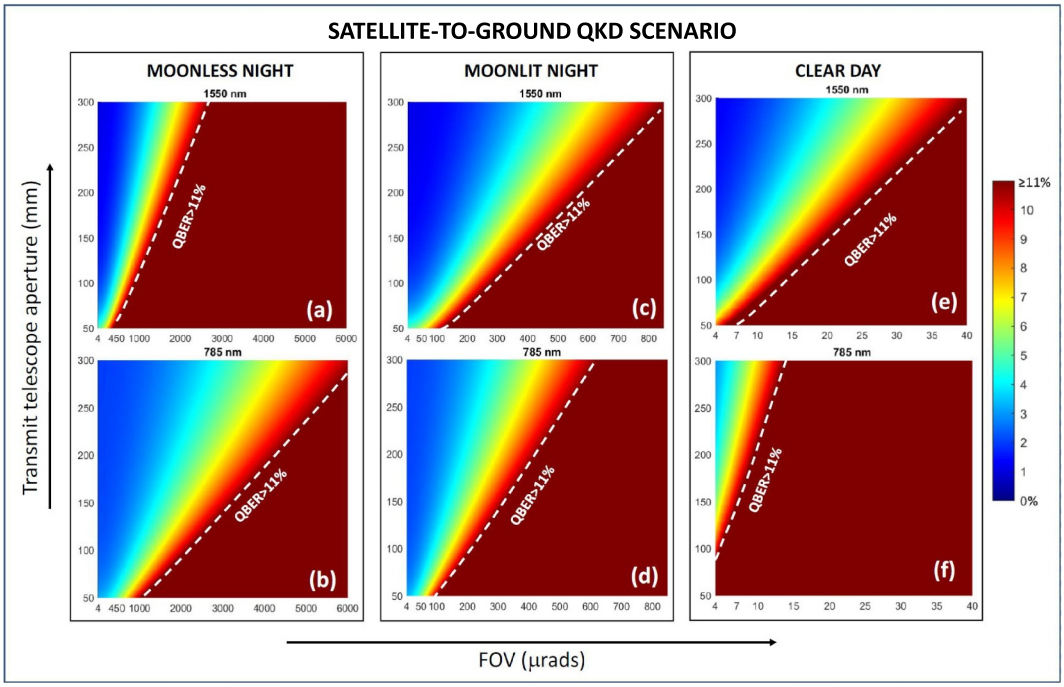

FIGURE 2 Estimated signal QBER for the satellite-to-ground QKD scenario; Moonless night condition: (a) 1550 nm and (b) 785 nm, Moonlit night condition: (c) 1550 nm and (d) 785 nm, Clear-day condition: (e) 1550 nm and (f) 785 nm.

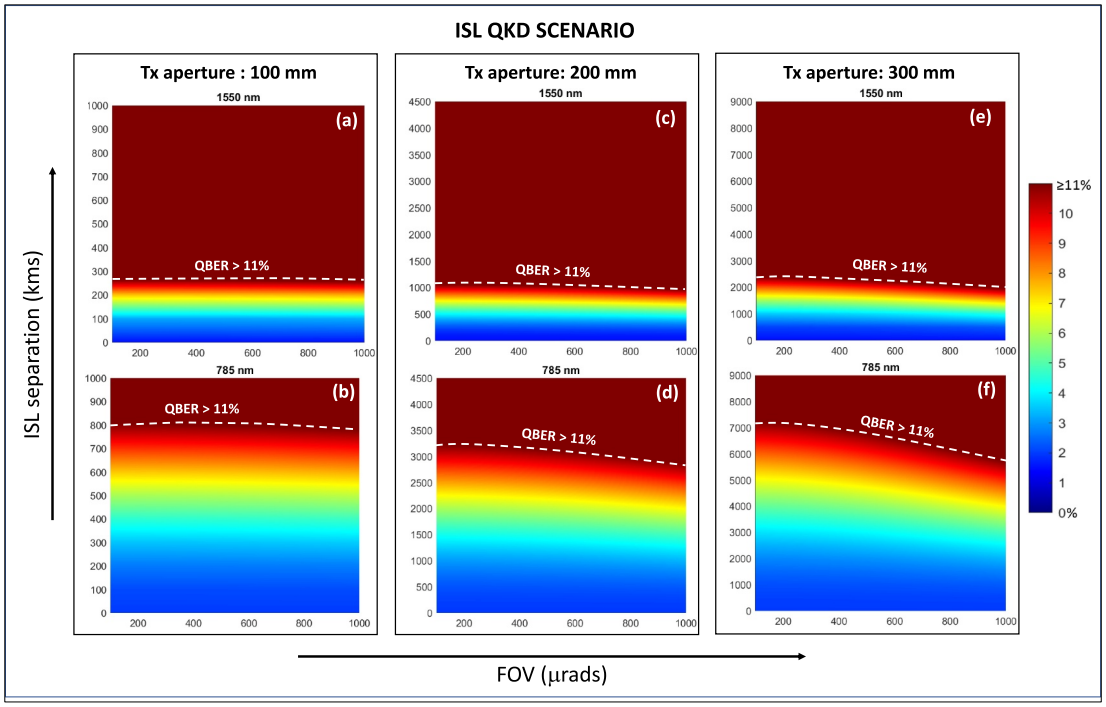

FIGURE 3 Estimated signal QBER for the ISL QKD scenario; 100 mm Tx aperture: (a) 1550 nm and (b) 785 nm; 200 mm Tx aperture: (c) 1550 nm and (d) 785 nm; 300 mm Tx aperture: (e) 1550 nm and (f) 785 nm.

It can be observed that with the transmit aperture size of 100 mm, the maximum separation for which 1550 nm ISL QKD is feasible with QBER <11% is 250 km, while for a larger aperture of 300 mm, the distance increases to 2000 km. With 785 nm, however, this maximum ISL separation range value gets increased to 750 and 6500 km for the 100 and 300 mm aperture, respectively. The primary reason for this increase is because of the near double transmit beam divergence experienced by a 1550 nm signal compared to the 785 nm, resulting in larger geometric path loss.

5 | ANALYSIS OF THE SYSTEM REQUIREMENTS FOR SATELLITE BASED QKD SCENARIOS

For a satellite-to-ground scenario with a 100 mm onboard telescope, it can be seen that for the moonless night operation scenario 785 nm performs better than 1550 nm, however for moonlit night scenario, the receiver FOV must be < 300 μrad and <250 μrad for 1550 and 785 nm, respectively, to ensure the QBER remains <11%. Even with 250 μrad as the FOV, the initial assumption of 3 dB pointing loss is acceptable as it corresponds to a pointing error of 7.5 μrad for 1550 nm and 3.9 μrad for 785 nm [34], which is much less than the FOV itself. However, when operating in daylight conditions with a 100 mm transmit aperture, the FOV must be <13 μrad for 1550 nm and <4.7 μrad for 785 nm. Correspondingly, the maximum stray noise the system can tolerate is 3.8×10^{-5} and 1.4×10^{-5} counts/pulse for 785 and 1550 nm, respectively. Thus, for moonlit night and clear-day conditions, the 1550 nm seems to be a better choice for QKD. Clearly, the pointing accuracy needs to be better than these stringent collecting FOV values in order to cater to daylight QKD scenarios.

For the case of ISL QKD, the use of 1550 nm appears more difficult to practically realise as it demands at least a 300 mm onboard telescope that leads to increase in payload mass, weight and power consumption. Similar performance can be realised using 785 nm with smaller transmit apertures of <200 mm. Also, from this analysis, it is evident that for the case where satellites are in sunlit condition, the system requirement such as minimum ISL separation and Tx aperture size will become even more demanding, making it unfeasible for practical realisation with current available technology.

Apart from FOV, certain device parameters can also be optimised to achieve lesser QBER with increased distance. Firstly, the telescope and associated optics need to be designed and fabricated such that the practical divergence is close to its theoretical diffraction limited value. Another parameter of interest could be the pulse width and pulse repetition frequency of the transmitter. Smaller pulse widths allow for smaller gating windows, whereas higher Pulse Repetition Frequency (PRF) would increase the signal photon detections, both of which help in improving the overall SNR. Other parameters for improving QBER performance include the front-end optics throughput as it is directly linked to the overall efficiency, spectral filter bandwidth (B_{filter}) of the receiver as the filter with smaller FWHM to further reduce the stray photons being captured by the OGS, and the use of adaptive optics at the OGS will reduce the influence of the atmospheric turbulence.

TABLE 2 Comparison of estimated QBER values with reported experimental works.

Operating conditions	Reference	Yo	Signal QBER
850 nm (night time only)	Measured results (Micius [12])	~ 5.89×10^{-7}	~3%
	Estimated [this work] ($H_b = 2 \times 10^{-7}$ $W.m^{-2}.Sr^{-1}.nm^{-1}$, B_{filter} = 10 nm, FOV = 20 μrad, P_{AP} = 2%)	~ 5.27×10^{-7}	2.8%
800 nm (night time only)	Measured results (SOCRATES [13])	~ 9×10^{-5}	~4.9%
	Estimated [this work] ($H_b = 5.25 \times 10^{-7}$ $W.m^{-2}.Sr^{-1}.nm^{-1}$, B_{filter} = 5 nm, FOV = 100 μrad, P_{AP} = 2%, e_{pol} = 3.5%, gating = 10 ns)	~ 9.18×10^{-5}	4.88%

Note: For estimating signal QBER, the operating conditions for the maximum QBER have been simulated. The assumed parameter values considered are mentioned in parenthesis for each section.

The accuracy of this developed QBER model would further improve if the experimentally measured sky radiance data around the concerned OGS region can be fed into it.

Y_o and signal QBER values were calculated using this developed model for two well-reported satellite-to-ground QKD experiments. We found the outcome of this model to be in good agreement with the published measured data as summarised in Table 2 [12, 13], thus validating the applicability of the developed model for practical scenarios. We also compared our model with one of the recent terrestrial free space daylight QKD experiment carried out at 1550 nm [25], and the estimated signal QBER of ~3.20% (for $H_b = 1.5 \times 10^{-3}$ $W.m^{-2}.Sr^{-1}.nm^{-1}$, $P_{AP} = 2\%$, $\eta_{op} = 75\%$) was also found to be in close agreement with the reported measured QBER of 3.24%. Further, our model was compared with our previously conducted inter-building free space QKD demonstration at 785 nm during night time over ~300 m [35], and the estimated signal QBER of ~2.5% (for $H_b = 1.4 \times 10^{-7}$ $W.m^{-2}.Sr^{-1}.nm^{-1}$—H_b was estimated based on the dark-noise measurement, $e_{pol} = 1.5\%$) was also found to be in close agreement with the reported measured QBER of ~2.6%.

6 | CONCLUSION

In this work, the main sources of noise encountered in the satellite-based quantum communication link and errors limiting the QBER performance of the satellite QKD system have been discussed and analysed. A more inclusive mathematical model of the QBER has been presented considering prime noise contributors such as stray light, polarisation errors, dark counts and after-pulsing effects. The influence of the various system parameters for the estimation of signal QBER in the satellite-to-ground downlink and ISL QKD scenarios have been investigated in detail. The simulation and comparative analysis for 800 and 1550 nm wavelength window are presented for different sky brightness conditions, which clearly shows the advantage of a 800 nm waveband for satellite-to-ground QKD during night time operation. However, for day time operation, 1550 nm window performs slightly better but poses stringent system requirements. Requirement analysis has also been presented for the design of various technology elements for space and ground segments in order to practically realise an efficient satellite-based QKD links while operating the system in a quantum secure regime. Also, the efficacy of this developed QBER model has been validated with measured results of the only reported satellite-to-ground QKD experiments as well as few recent terrestrial free space experiments.

AUTHOR CONTRIBUTIONS

All the authors have contributed equally.

ACKNOWLEDGEMENTS

The authors would like to acknowledge Shri. Nilesh M Desai, Director, SAC, for encouragement, guidance and continuous support to this work. The authors would also like to acknowledge their colleague Dr. Manoj Mishra for valuable discussions on sky brightness and background noise.

CONFLICT OF INTEREST STATEMENT

The authors declare no potential conflict of interests.

DATA AVAILABILITY STATEMENT

The data that supports the findings of this study are available from the corresponding author upon reasonable request.

ORCID

Abhishek Khanna https://orcid.org/0000-0001-7595-4173

REFERENCES

1. Gisin, N., et al.: Quantum cryptography. Rev. Mod. 74(1), 145–195 (2002). https://doi.org/10.1103/revmodphys.74.145
2. Bennett, C.H., Brassard, G.: Quantum Cryptography: Public Key Distribution and Coin Tossing (2020). arXiv preprint arXiv:2003.06557
3. Bennett, C.H., et al.: Experimental quantum cryptography. J. Cryptol. 5(1), 3–28 (1992). https://doi.org/10.1007/bf00191318
4. Bennett, C.H.: Quantum cryptography using any two nonorthogonal states. Phys. Rev. Lett. 68(21), 3121–3124 (1992). https://doi.org/10.1103/physrevlett.68.3121
5. Lounis, B., Orrit, M.: Single-photon sources. Rep. Prog. Phys. 68(5), 1129–1179 (2005). https://doi.org/10.1088/0034-4885/68/5/r04

6. Hadfield, R.H.: Single-photon detectors for optical quantum information applications. Nat. Photonics 3(12), 696–705 (2009). https://doi.org/10.1038/nphoton.2009.230
7. Yin, H.L., et al.: Measurement-device-independent quantum key distribution over a 404 km optical fiber. Phys. Rev. Lett. 117(19), 190501 (2016). https://doi.org/10.1103/physrevlett.117.190501
8. Ecker, S., et al.: Strategies for achieving high key rates in satellite-based QKD. npj Quan. Inf. 7(1), 5 (2021). https://doi.org/10.1038/s41534-020-00335-5
9. Dequal, D., et al.: Feasibility of satellite-to-ground continuous-variable quantum key distribution. npj Quan. Inf. 7(1), 3 (2021). https://doi.org/10.1038/s41534-020-00336-4
10. Bonato, C., et al.: Feasibility of satellite quantum key distribution. New J. Phys. 11(4), 045017 (2009). https://doi.org/10.1088/1367-2630/11/4/045017
11. Bedington, R., Arrazola, J.M., Ling, A.: Progress in satellite quantum key distribution. npj Quan. Inf. 3(1), 30 (2017). https://doi.org/10.1038/s41534-017-0031-5
12. Liao, S.K., et al.: Satellite-to-ground quantum key distribution. Nature 549(7670), 43–47 (2017). https://doi.org/10.1038/nature23655
13. Takenaka, H., et al.: Satellite-to-ground quantum-limited communication using a 50-kg-class microsatellite. Nat. Photonics 11(8), 502–508 (2017). https://doi.org/10.1038/nphoton.2017.107
14. Ntanos, A., et al.: Leo satellites constellation-to-ground QKD links: Greek quantum communication infrastructure paradigm. Photonics 8(12), 544 (2021). https://doi.org/10.3390/photonics8120544
15. Podmore, H., et al.: QKD Terminal for Canada's Quantum Encryption and Science Satellite (QEYSSat), pp. 203–212. SPIE (2021).11852
16. Kerstel, E., et al.: Nanobob: a CubeSat mission concept for quantum communication experiments in an uplink configuration. EPJ Quan. Technol. 5(1), 6 (2018). https://doi.org/10.1140/epjqt/s40507-018-0070-7
17. Lütkenhaus, N.: Estimates for practical quantum cryptography. Phys. Rev. 59(5), 3301–3319 (1999). https://doi.org/10.1103/physreva.59.3301
18. Gruneisen, M.T., et al.: Modeling daytime sky access for a satellite quantum key distribution downlink. Opt Express 23(18), 23924–23934 (2015). https://doi.org/10.1364/oe.23.023924
19. Li, H.W., et al.: Improving the performance of practical decoy-state quantum key distribution with advantage distillation technology. Commun. Phys. 5(1), 53 (2022). https://doi.org/10.1038/s42005-022-00831-4
20. Klop, W., et al.: QKD Optical Ground Terminal Developments, pp. 388–403. SPIE (2021).11852
21. Tan, Y., Cai, Q.: Practical decoy state quantum key distribution with finite resource. The Eur. Phys. J. D 56(3), 449–455 (2010). https://doi.org/10.1140/epjd/e2009-00316-1
22. Ma, X., et al.: Practical decoy state for quantum key distribution. Phys. Rev. 72(1), 012326 (2005). https://doi.org/10.1103/physreva.72.012326
23. Wu, J., et al.: Polarization-maintaining design for satellite-based quantum communication terminals. Opt Express 28(8), 10746–10759 (2020). https://doi.org/10.1364/oe.387574
24. Mushtaq, M., et al.: Analysis of internal design parameters to minimize geometrical losses in free-space optical communication link. Acta Phys. Pol. A. 134(1), 275–277 (2018). https://doi.org/10.12693/aphyspola.134.275
25. Liao, S.K., et al.: Long-distance free-space quantum key distribution in daylight towards inter-satellite communication. Nat. Photonics 11(8), 509–513 (2017). https://doi.org/10.1038/nphoton.2017.116
26. Papapanos, C., et al.: Afterpulsing Effect on the Baseline System Error Rate and on the Decoy-State Quantum Key Distribution Protocols (2020). arXiv preprint arXiv:2010.03358
27. Er-Long, M., et al.: Guang-Can G. Background noise of satellite-to-ground quantum key distribution. New J. Phys. 7(1), 215 (2005). https://doi.org/10.1088/1367-2630/7/1/215
28. ExcelitasTechnologies: PHOTON COUNTING MODULE. SPCM-780-14-FC datasheet.Rev 2020-04
29. IDQuantique: ID281 Superconducting Nanowire Series. datasheet (2022)
30. Alluxa: Alluxa Product Line – Ultra Narrow Band-Pass Filter. datasheet (accessed Dec 2022)
31. Yao, N., et al.: Optimizing up-conversion single-photon detectors for quantum key distribution. Opt Express 28(17), 25123–25133 (2020). https://doi.org/10.1364/oe.397767
32. Ma, F., et al.: Upconversion single-photon detectors based on integrated periodically poled lithium niobate waveguides. JOSA B 35(9), 2096–2101 (2018). https://doi.org/10.1364/josab.35.002096
33. Bai, P., Zhang, Y., Shen, W.: Infrared single photon detector based on optical up-converter at 1550 nm. Sci. Rep. 7(1), 15341 (2017). https://doi.org/10.1038/s41598-017-15613-0
34. Marshall, W.K.: Transmitter pointing loss calculation for free-space optical communications link analyses. Appl. Opt. 26(11), 2055 (1987). https://doi.org/10.1364/ao.26.2055_1
35. Jain, A., et al.: Development of NavIC synchronized fully automated inter-building QKD framework and demonstration of quantum secured video calling. Optik 252, 168438 (2022). https://doi.org/10.1016/j.ijleo.2021.168438

How to cite this article: Khanna, A., et al.: Quantum BER estimation modelling and analysis for satellite-based quantum key distribution scenarios. IET Quant. Comm. 5(2), 157–163 (2024). https://doi.org/10.1049/qtc2.12081